

Narrow-Band Emission Line Imaging with NICMOS: Lessons Learned from the Data Reduction of OMC-1

Susan R. Stolovy

Steward Observatory, University of Arizona, Tucson, AZ, 85721

Abstract. Narrow-band emission-line imaging with NICMOS is discussed, with an emphasis on what has been learned from the data reduction of the molecular hydrogen imaging of OMC-1 with Camera 2. Issues discussed here include: continuum subtraction, photometry, electronic ghosts, and mosaicking images with different sky orientations.

1. Continuum Subtraction

Accurate continuum subtraction is clearly a crucial step to obtaining a pure line image. For this reason, pairs of narrow-band filters have been provided in NICMOS to image such astrophysically interesting lines as: HeI (F108N/F113N), [FeII] (F164N/F166N), Pa α (F187N/F190N), [SiV] (F196N/F200N), H₂ (F212N/F215N), and Br γ (F216N/F215N). The discussion here is based on the Early Release Observations (ERO) of the Orion Molecular Cloud (OMC-1) in H₂ taken on April 12–13, 1997. (Stolovy et al. 1997).

1.1. Relative Photometry

Table 1 shows a comparison of five different methods of determining the *relative* flux calibration for the two narrow-band filters F212N and F215N for Camera 2. None of these assumes any prior (ground-based) knowledge of the absolute flux of the astronomical object. These methods were remarkably consistent. A multiplicative factor of 1.10 was adopted to normalize the F215N filter to the F212N transmission.

Table 1. Relative Photometry of Filters ^a

Method	F212N	F215N	Ratio (215/212)
Absolute Flux (P330E)	4.07×10^{-5} Jy/ADU/s	4.48×10^{-5} Jy/ADU/s	1.10
Flat Field Avg. Count Rate	29.8 ADU/s	26.6 ADU/s	1.12
Photometry Header Keyword PHOTFNU	4.97×10^{-5} Jy/ADU/s	5.49×10^{-5} Jy/ADU/s	1.10
Median in ‘blank’ part of OMC-1 ^b	0.517 ADU/s	0.475 ADU/s	1.07
Exposure Time Calculator (S/N) ^c			1.08

^aAll values rounded to 3 significant figures

^bMedian over 400 pixels in area with minimal H₂ emission; Typical 1- σ for ratio is 0.05

^cRatio based on signal/noise estimates for fluxes ranging from 1mJy to 1 Jy, exposure times chosen to give S/N \geq 100

1.2. Absolute Photometry

The absolute photometry was based on observations of the standard star and solar analog, P330E. This star was observed in many NICMOS filters, although not in F212N and F215N.

The spectrum of P330E is sufficiently well-known that, in conjunction with known filter response curves and flat fields, the error in characterizing the standard star spectrum (and translating that to photometry in the NICMOS filters) is estimated to be accurate to better than 5% (M. Rieke, private communication). However, the absolute photometry derived from observations of P330E have been updated several times since the Orion observations in April. The header keyword values (e.g. PHOTFNU, PHOTFLAM) have changed quite drastically since these very early observations in April, and we caution observers to employ independent methods of absolute flux calibration if possible. There is some evidence of time-dependent photometric behavior in NICMOS, which has yet to be fully understood. The current estimate of absolute photometry accuracy is 10–15% (Colina & Rieke 1997).

We have also done a rough comparison of the adopted absolute photometry with both ground-based continuum (K-band at 2.2 μm) and H_2 (with 1.5'' resolution). Both were consistent to within the rather large errors of the ground-based measurements ($\pm 15\%$). In a field full of bright, extended emission as well as crowding from stars, one must first degrade the NICMOS image to the equivalent beam size of ground-based images to truly compare the photometry. This has yet to be done in detail; at this point, the absolute photometry of highly saturated sources in NICMOS images (such as BN in the OMC–1 image) is suspect, but all other objects should be valid to an estimated 15%.

2. Linearity and Persistence

At the time of observation, it was clear that the “calnica” reduction software was not properly correcting non-linear responses of some pixels, which appeared as low values near the centers of moderately bright stars and in the first Airy ring for highly saturated stars. We interpreted this as a failure of the linearity reference file to flag non-linear pixels early enough during the onset of saturation, when the count rate displays a marked decrease. To correct this, the linearity reference file was modified by multiplying by 0.95 to lower the threshold for saturation flagging. This appeared to work to first order, but the preferred algorithm for linearity correction is still work in progress, including the effects of high count rates in the “zeroth” read.

Persistence must be present in those pixels that are saturated or near saturation. However, since no dithers were done during an orbit (although a change in filter was made), there is no way to observe latent images directly from the OMC–1 data. There was no clear signature of persistence between the last observation of the bright star BN (which saturated in 3 seconds) and the first observation of the new target, about 1 hour later. We hope to model persistence characterized by other observations (with dithers) in order to estimate the effects on photometry of bright objects. Latent images in such a dither pattern have recently been observed in darks taken after observing saturated sources even 30 minutes after exposure.

3. Seeing Ghosts

It is now well-known that “electronic ghosts” appear one quadrant (128 pixels) away from saturated pixels due to electrical crosstalk between detector quadrants. For especially bright sources, a “stripe” spanning two adjacent quadrants is seen along the readout direction where the bright source is located as well as 128 pixels away in the other 2 quadrants. This is often a very subtle effect (with signal levels for the “ghost” typically ≥ 1000 times fainter than the bright object), but an important one in assessing the validity of faint sources in a field such as OMC–1. For instance, a faint source located near the suspected outflow source ‘I’ thought to power the molecular outflow in OMC–1 was observed in two overlapping frames (see Stolovy et al. 1997). In one pointing, a bright star was located exactly 128 pixels away, but no such star was present in the other pointing, where the faint source was

weaker in flux. Therefore, this object of intrinsic scientific interest is part real and part electronic ghost!

It has yet to be determined if optical ghosts (caused by reflections) exist in NICMOS images. Latent images can mimic in-focus optical ghosts as seen in the FOM test (proposal 7156) where a bright star is moved around on the detector.

4. Orientation Considerations

For these ERO observations, no ORIENT constraint was given between visits. Each visit was an orbit, and the SAME ORIENT in RPS2 should have been used to force the different visits to have the same sky orientation. This complicates the analysis and mosaicking of NICMOS images in several ways, as discussed below. These are listed as a caveat to others who might either inadvertently or purposefully (for instance, in the case of roll angle changes for coronagraphic observations) obtain spatially overlapping NICMOS data with different sky orientations. The maximum change in orientation between the 5 orbits of the OMC-1 data was ~ 4.5 degrees.

- Each image must be rotated according to orientation in header before mosaicking. Note that header parameter ORIENTAT is the angle required to rotate the image by to get north up; e.g., if ORIENTAT = -120 , rotate the image clockwise 120 degrees. The IRAF routine `rotate` with cubic spline interpolation was used, which inevitably smooths the data slightly.
- The spatial coverage was not as complete as it would have been with a constant orientation.
- Diffraction patterns are fixed relative to detector coordinates, so patterns will not match up if overlapping frames have different orientations. Note that diffraction patterns from nearby bright stars are not attenuated when star is off detector. (BN's diffraction spikes can be seen more than $20''$ from the star's centroid!)
- If deconvolution is used, each image must be deconvolved with *unrotated* images so that the diffraction pattern of the PSF matches the data. If each image is part of a mosaic with large overlaps between frames of different orientations, the S/N will be compromised, as the mosaic cannot be deconvolved.

5. Construction of F212N, F215N and H₂ Mosaics

A mosaic routine written in IDL was used to assemble the OMC-1 images. It accepts a list of offsets determined by centroids on stars common to both images or one can "blink" images by eye to align and produce the offset list (this is especially useful for diffuse features). The mosaic procedure keeps track of statistical weights for each pixel and replaces bad with good pixels if there is overlap. Each image was corrected for the aspect ratio of the plate scale and was then rotated so that north was up and east to the left before mosaicking. The plate scale, determined on April 17 (a few days after the observations), was $0.076320''/\text{pix}$ in x and $0.075655''/\text{pix}$ in y. The 256×256 pixel images were rebinned to 516×511 images to correct the non-square aspect ratio and to allow for a more accurate registration of spatially overlapping images. The F212N and F215 mosaics were produced with identical rotations and offsets. The resulting alignment accuracy is better than $0.02''$ (half of the small pixel size). The mosaics were then rebinned by a factor of two to approximate the size of original detector pixels, producing square pixels with a plate scale of $0.07577''/\text{pix}$. The effects on point-spread functions due to rotation and rebinning caused a minimal amount

of broadening (less than 3% FWHM). Each mosaic was then converted to Jy/pixel using the absolute conversion factors listed above derived from the P330-E model.

In order to produce a pure H₂ line image, the flux-calibrated F215N image needs to be subtracted from the F212N image. It became apparent that there was a shift in the centroids of stars in the two mosaics. A shift of ≈ 0.2 pixels was necessary in order to align the mosaics, which was done with the IRAF routine `imshift`. This rather large shift (twice the rms jitter of 7 mas) may have been partly explained by ill-defined apertures during the ERO phase; the targets were not in the center of the array, which could have introduced a small tracking error. Whether such shifts are caused by pointing shifts or filter optics, they will likely be present at small levels for narrow-band imaging. A shift as small as 0.02 pixels (Camera 2) is evident in comparing subtracted images.

As a sanity check on the correct subtraction of F215N from F212N, the relatively “blank” areas of the OMC-1 mosaic do indeed have a median value near zero (the median is of order 1.3×10^{-6} Jy/pix or $\sim 2\sigma$ in the subtracted image). Some of the stars in the H₂ image also have a median (or mean) integrated value near zero, but others, including BN, are distinctly negative. Since H₂ is essentially never optically thick (i.e. it’s never seen in absorption), we interpret these “negative” stars as being so red that they are intrinsically brighter at F215N than F212N. In the case of BN, it is measured to be 17% brighter at F215N. However, the effects of persistent images accumulating in the F215N filter (taken after the F212N in the same orbit) need to be explored more carefully.

Acknowledgments. I would like to acknowledge Marcia Rieke for her insightful discussions and careful assessment of NICMOS performance.

References

- Colina, L. & Rieke, M., 1997, this volume.
Stolovy, S. R., Burton, M. G., Erickson, E.F., Kaufman, M.J., Chrysostomou, A., Young, E.T., Colgan, S.W.J., Axon, D.J., Thompson, R.I., Rieke M.J., and Schneider, G. 1997 ApJ Letters (in press).

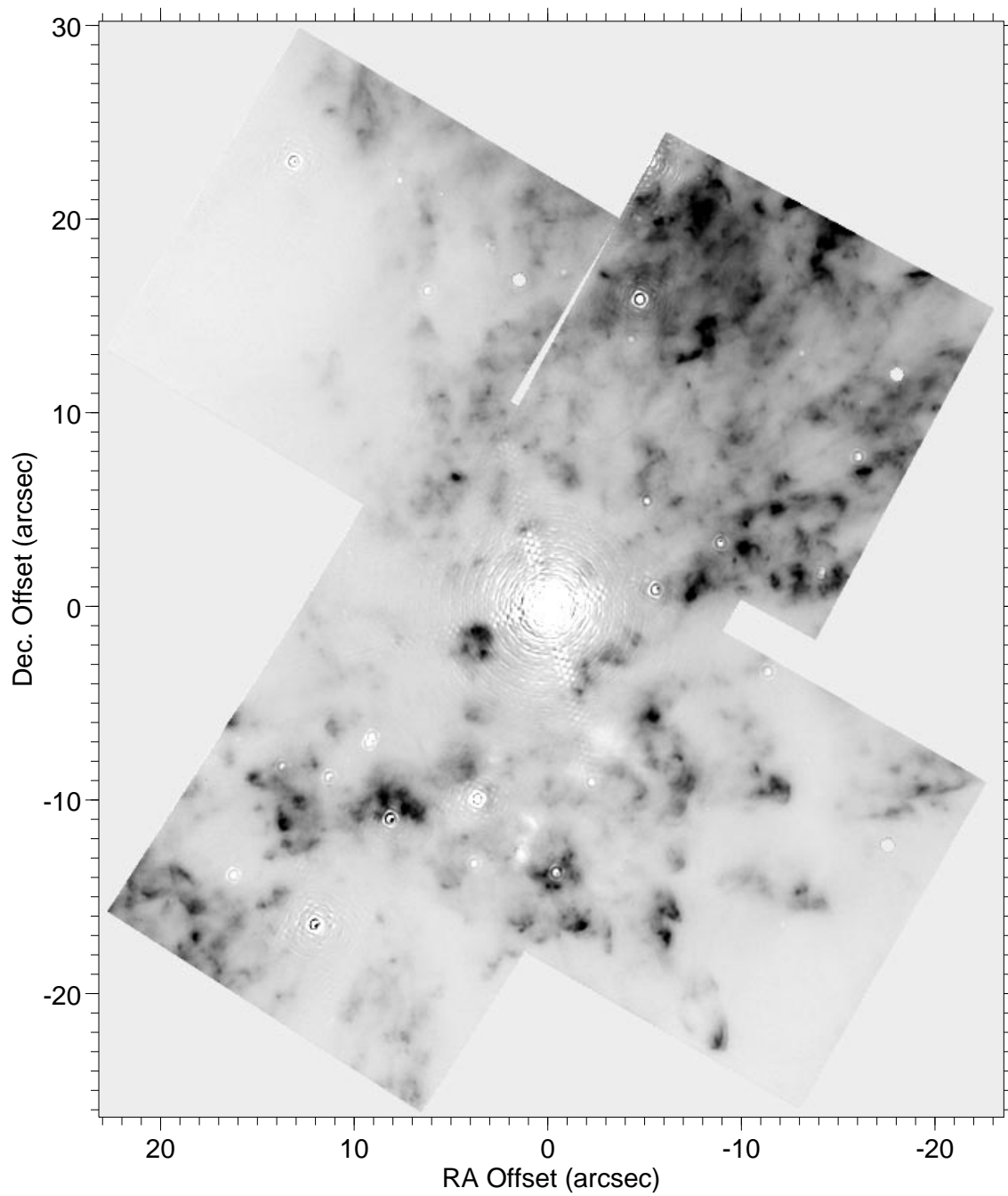


Figure 1. Molecular hydrogen mosaic of the core of OMC-1 in the $2.12\mu\text{m}$ line, adapted from Stolovy et al. (1997). The gray scale is linear, increasing from white to black.